Showcasing research from Professor Arges's and Dr. Lin's laboratory, Cain Department of Chemical Engineering and the Applied Materials Division, Louisiana State University and Argonne National Laboratory, USA.

Promoting water-splitting in Janus bipolar ion-exchange resin wafers for electrodeionization

Promoting water-splitting in Janus bipolar ion-exchange resin wafers for electrodeionization. This image conveys a new class of Janus bipolar resin wafer for electrodeionization – an electrified water treatment process. The work investigated how an incorporated water dissociation catalyst, the pearl colored spheres between the layers in the image, in the Janus bipolar resin wafer regenerates the ion-exchange resins while augmenting the ionic conductivity during deionization. The new porous ionic conductors will be useful for water treatment applications that require pH adjustment – such as silica and organic acid removal.

As featured in:

See Yupo J. Lin, Christopher G. Arges *et al.*, *Mol. Syst. Des. Eng.*, 2020, **5**, 922.

ROYAL SOCIETY OF CHEMISTRY

rsc.li/molecular-engineering

PAPER

Check for updates

Promoting water-splitting in Janus bipolar ion-exchange resin wafers for electrodeionization†

Matthew L. Jordan, ‡[a] Lauren Valentino, ‡[b] Nargiza Nazyrynbekova, [a] Varada Menon Palakkal, [a] Subarna Kole, [a] Deepra Bhattacharya, [a] Yupo J. Lin *[b] and Christopher G. Arges *[a]

Electrochemical separation processes are undergoing a renaissance as the range of applications continues to expand because they offer opportunities for increased energy efficiency and sustainability in comparison to conventional separation technologies. Existing platforms such as electrodialysis and electrodeionization (EDI) are seeing significant improvement and are currently being deployed for treating a diverse set of liquid streams (*e.g.*, water and wastewater treatment, organic acid separation, *etc.*). In addition, the relatively low inherent electricity requirement for electrochemical separations could potentially be satisfied through integration with sustainable sources of renewable energy. In order to achieve a truly sustainable electrochemical separations process, it is paramount to improve the energy efficiency of electrochemical separations by minimizing all sources of resistances within these units. This work reports of a new class of symmetric and asymmetric Janus bipolar resin wafers (RWs) that augment the spacer channel ionic conductivity in EDI while having the additional functionality of splitting water into protons and hydroxide ions. The latter attribute is important in niche applications that require pH modulation such as silica and organic acid removal from liquid streams. The Janus bipolar RWs were devised from single ion-conducting RWs that were interfaced together to create an intimate polycation–polyanion junction. Interestingly, the conductivity of the single ion-conducting RWs at low salt concentrations was observed to be dependent on the ionic mobilities of the counterions that the RW was transferring. Using single ion-conducting RWs to construct Janus bipolar RWs enabled the incorporation of a water-splitting catalyst (aluminum hydroxide nanoparticles) into the porous ion-exchange resin bed. To the best of our knowledge, this is the first time a water dissociation catalyst has been implemented in the ion-exchange resin bed for EDI. The water dissociation catalyst in bipolar junctions pre-polarizes water making it easier to split into hydronium and hydroxide ion charge carriers under applied electric fields *via* the second Wien effect. The new molecularly layered Janus RWs demonstrate both satisfactory water-splitting and salt removal in bench scale EDI setups and these materials may improve, or even supplant, existing bipolar membrane electrodialysis units that currently necessitate large electrolyte feed concentrations.

Design, System, Application

Bipolar membranes are the standard-bearer material for pH adjusting process streams without the addition of acids and bases in electrodialysis. These membranes feature weak-acid or -base catalysts that pre-polarize water at the polycation–polyanion interfaces making it susceptible for splitting into hydronium and hydroxide ion charge carriers under electric fields. Further, they require intimate polycation–polyanion interfaces as large distances between the fixed charges compromise water-splitting efficiency. A limitation of bipolar membrane electrodialysis (BPMED) is the need for concentrated salt feeds to overcome significant ohmic resistances in the diluate chamber. This work engineered a new class of porous, Janus ion-exchange resin wafers (RWs) featuring bipolar junctions with aluminum hydroxide (Al(OH)$_3$) nanoparticles as the water dissociation catalyst. These RWs have a flexible material design as the Al(OH)$_3$ catalyst can be incorporated into different layers and can have tuned polycation–polyanion molecular interfaces through application of thin film ionomer coatings. The Janus bipolar RWs augmented the diluate chamber ionic conductivity in electrodeionization (EDI) setups, overcoming limitations experienced in BPMED, while also co-currently splitting water and removing chloride ions. It is envisioned that the Janus bipolar RWs will be useful in niche water treatment applications that require pH adjustment – *e.g.*, silica and organic acid removal.

[a] *Cain Department of Chemical Engineering, Louisiana State University, Baton Rouge, LA 70803, USA. E-mail: carges@lsu.edu*
[b] *Applied Materials Division, Argonne National Laboratory, Lemont, IL 60439, USA. E-mail: yplin@anl.gov*

922 | *Mol. Syst. Des. Eng.*, 2020, 5, 922–935

This journal is © The Royal Society of Chemistry 2020

Introduction

Separation processes are integral operations to chemical and industrial plants, and they play a prominent role in the economics and quality of products for chemical, pharmaceutical, food, and biotechnological applications. On average, 40% of operation costs and 40% of capital costs for chemical plants are attributed to separation processes,[1] and a 2019 United States National Academy Report[2] highlighted that 10 to 15% of all U.S. energy production is consumed by separation processes. Conventional separation methods including distillation, evaporation, and crystallization require a phase change and are energy intensive. The corresponding economic costs and environmental concerns about fossil-fuel emissions are driving the research and development of more energy-efficient and cost-effective separation processes and technologies. At the forefront of more efficient, modular, and selective separations, are molecularly engineered material deployed in membrane-based and adsorbent-based separations. Undoubtedly, new materials and maturation of emerging separation platforms that are less energy intensive will be at the forefront of future separations technologies.

An important sub-subset of separations relates to electrochemical systems that are effective for removing ionic species from aqueous and non-aqueous liquids. Such processes are used in industrial wastewater remediation and deionization. Electrochemical systems for ionic species removal from liquid streams include well-established platforms such as electrodialysis (ED)[3] and electrodeionization (EDI)[4–7] and emerging ones such as membrane capacitive deionization/capacitive deionization (MCDI/CDI)[8–11] and shock electrodialysis.[12,13] Electrochemical separations have also been used for purifying gases through electro-swing reactive[14] and RW-EDI gas adsorption.[15]

A key component for realizing high energy efficiency and high performance in electrochemical separations is minimizing sources of resistance through adjustment of the system's operating parameters and implementation of new materials. For example, Lin *et al.* were able to optimize the system parameters (*e.g.*, cell voltage and feed concentration flow rate) for RW-EDI to make it more energy efficient than reverse-osmosis (RO) for brackish water treatment (2000 ppm of total dissolved solids (TDS) to 5000 ppm of TDS in the feed concentration).[16] As a materials example, Palakkal *et al.* showed that reducing the ion-exchange membrane (IEM) materials' area-specific resistance (ASR) by a factor of 5 to 10 resulted in a 50% reduction in energy consumption for desalination at low TDS concentrations (*e.g.*, 250 ppm to 540 ppm).[17] Hence, both materials innovation and systems level engineering enhanced energy efficiency for electrochemical separations.

A uniquely defining phenomenon in the EDI process is the regeneration of the ion-exchange resin beads during deionization through water-splitting. Unlike ion-exchange chromatography, EDI can be implemented as a continuous ion-exchange process because water-splitting, which results in the formation of hydroxide (OH^-) ions and protons (H^+), occurs in the ion-exchange resin bed. These ions can exchange back into the anion exchange and cation exchange resin (AER and CER) particles, respectively, recombine to form water, or migrate out of the diluate chamber *via* the anion exchange and cation exchange membranes (AEMs and CEMs). Hence, the water-splitting phenomenon allows for continuous ion-exchange and removal of charged species from the liquid feed stream. Ion-exchange chromatography, on the other hand, requires acid and base chemicals for regenerating the ion-exchange resin particles in the column. The use of these chemicals leads to undesirable waste, downtime for the regeneration/cleaning process, and higher capital costs because multiple columns need to be installed in parallel to ensure a continuous process.

Water-splitting in EDI has been well-documented;[4,18] however, it has been primarily discerned by monitoring the pH changes of the effluent streams. In a continuous EDI process (see Fig. 1A), the ions in the aqueous solution are adsorbed *via* ion-exchange onto the resin beads. These adsorbed ions are then successively desorbed from the adsorption sites by two parallel phenomena: i.) electrically-driven migration and ii.) resin bead regeneration caused by H^+ and OH^- ions that are generated from water-splitting. More specifically, the desorbed salt ions exchanged by the OH^- and H^+ ions electro-migrate into the concentrate compartment, which is separated by the ion-exchange membranes. At steady-state, there is constant concentration profile along the direction of feed flow for ions adsorbed on the ion-exchange resin beads to the ion-exchange membrane surfaces. In a continuous EDI process, the bulk of deionization occurs at the entrance to the middle region of the unit. As the concentration of mobile ions in the diluate stream decreases, the ion-exchange bed augments the diluate stream conductivity. Finally, water-splitting at the middle to the end of the chamber regenerates the ion-exchange resin particles and provides ions to enable electrical current flow through the EDI unit despite the majority of salt ions already being removed.[4,19]

The water-splitting phenomenon in EDI occurs at the interface of CER and AER particles that are in intimate contact and form a p–n type abrupt junction.[20] This junction of interfaced polycations and polyanions is designated as the bipolar junction (highlighted in Fig. 1B). Applying an external electric field gradient across the bipolar junction interface leads to water-splitting.[21] It is important to note that the depletion width for bipolar junction interfaces is few nanometers.[22] Therefore, large distances between the oppositely charged particles hinder water-splitting in the ion-exchange resin beds of EDI. Further, a small population of bipolar junctions in the ion-exchange resin particle bed minimizes the water-splitting effect leading to poor regeneration of ion-exchange resin particles. Conversely, increasing the number of bipolar junctions within the RW accelerates proton and hydroxide formation. Regardless of the electrochemical separation process, the water-splitting

This journal is © The Royal Society of Chemistry 2020

Mol. Syst. Des. Eng., 2020, **5**, 922–935 | 923
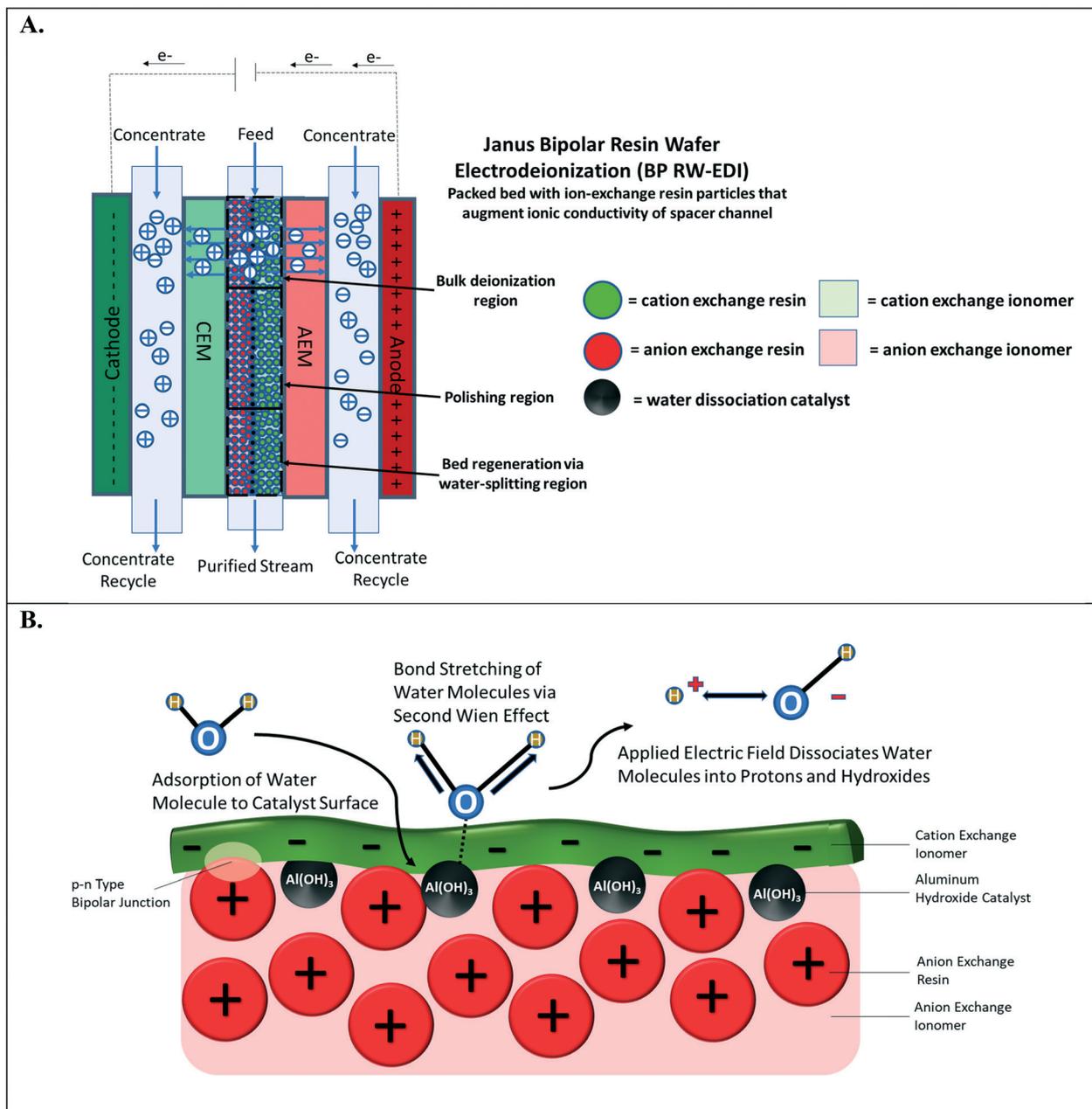
Fig. 1 (A) Depiction of a simplified Janus bipolar resin wafer electrodeionization (BP-RW EDI) process that has the bulk of deionization occurring at the inlet of the diluate chamber, followed by ion polishing in the middle of the chamber, and then water-splitting near the middle to the end of the diluate chamber to sustain current flow and to regenerate the ion-exchange resin particles. (B) Water dissociation at the metal hydroxide interface (*i.e.*, water dissociation catalyst) imbedded in an asymmetric Janus bipolar RW.

generated in the resin bed can be exploited to achieve a desired pH adjustment of the process stream (*e.g.*, during deionization, electrocoagulation of metals[23] and silica,[24] gas capture,[15] and mineral acid and base production[25,26]). For example, the maintenance of an alkaline solution can ensure that organic acids remain in ionized form for separation based upon anion exchange; this is important for carbon valorization and purifying bio-fuels.[27] BPM electrodialysis[25,26] has been the most common method for electrochemical pH adjustment of process streams, but this method necessitates

fairly concentrated streams of TDS to overcome spacer channel ohmic resistances to electrochemically transport the ions.

This paper, for the first time, demonstrates the incorporation of a water dissociation catalyst into ion-exchange RWs for promoting water-splitting in RW-EDI. Water dissociation catalysts, which are found in bipolar membranes, facilitate water-splitting *via* the second Wien effect[28] (depicted in Fig. 1B). The catalyst in the bipolar junction pre-polarizes water to severe its HO–H bond.

924 | *Mol. Syst. Des. Eng.*, 2020, **5**, 922–935

This journal is © The Royal Society of Chemistry 2020

Mallouk and co-workers[29] recently reported that the catalyst can dampen the strength of the electric field in the bipolar junction region for splitting water, but this undesired attribute is overshadowed by the importance of the catalyst that promotes water-splitting kinetics by several orders of magnitude – when compared to a bipolar junction with no catalyst. A previous effort[30] by our group attempted to incorporate a water dissociation catalyst[31,32] into immobilized ion-exchange RW used in EDI was unsuccessful as incorporation of the aluminum hydroxide (Al(OH)$_3$) nanoparticles, a water dissociation catalyst, compromised the mechanical integrity of the RW. To overcome this challenge, a layered manufacturing approach was adopted by 1) preparing a single ion-conducting RW, 2) depositing of Al(OH)$_3$, and 3) adjoining oppositely charged, single ion-conducting RW or a thin layer of oppositely charged ionomer film. These designs are termed symmetric Janus bipolar RW and asymmetric film Janus bipolar RW, respectively.

Prior to investigating the water-splitting behavior of the Janus bipolar RWs, the ionic conductivity of the single ion-conducting RWs were studied. Both single ion-conducting RWs featured an ionomer binder, and these wafers showed superior ionic conductivity over the RW that consisted of mixed AER and CER and a PE binder (*i.e.*, the benchmark material used at Argonne National Laboratory). The anion exchange ionomer (AEI) binder with AER RW (AEI–AER RW) displayed the highest ionic conductivity to date of all RW materials reported in the literature[16,30,33] (17 ± 0.3 mS cm^{-1} at 0.1 g L^{-1} in NaCl to 58 ± 3.6 mS cm^{-1} at 29 g L^{-1}). Interestingly, the CEI binder with CER RW (CEI–CER RW) exhibited lower ionic conductivity in comparison to the AEI–AER RW. Furthermore, addition of CER to AEI binder RW (AEI–CER RW) also resulted in lower ionic conductivity in comparison to the AEI–AER RW. These observations are primarily attributed to the lower ionic mobility of the Na$^+$ counterion in the CER when compared to the Cl$^-$ counterion in the AER. Hence, the ionic conductivity is largely influenced by both the ion-exchange resins and the ionomer binder.

With the newly prepared single ion-conducting RWs, the water-splitting behavior of the RWs with and without a water dissociation catalyst and different configurations (*e.g.*, symmetric and asymmetric) were studied. The incorporation of a water dissociation catalyst improved water splitting by factor of 2–4 while providing a similar level of ionic conductivity and porosity in comparison to the RWs without the catalyst. The Janus bipolar RW with a water dissociation catalyst caused significant pH shifts in the diluate and concentrate compartments of EDI that are similar to what is observed in bipolar membrane electrodialysis.[25,26] The Janus bipolar RW is an alternative material for pH adjustment of the concentrate and diluate streams in EDI rather than using a BPM. Notably, it can have tailored molecular interfaces located at different junctions across the wafer thickness for modulating pH adjustment of streams to different values.

Experimental

The methods to synthesize sulfonated poly(arylene ether ether ketone) (SPEEK) and quaternary benzyl *n*-methyl pyrrolidinium poly(arylene ether sulfone) (QAPSf) are documented in our previous works.[17,30,34] Specifications for the materials used in this study and the preparation of the conventional (benchmark PE-mixed) RW are provided in the supplemental information.

Static ionic conductivity (κ)

Electrochemical impedance spectroscopy (EIS) measurements were conducted on a Gamry 3000 AE Potentiostat operated in galvanostatic mode. A 2-point probe method was used with a cell consisting of 2 platinum foil working electrodes adhered to 2 adjustable stainless-steel collectors in a polytetrafluoroethylene (PTFE) housing. A stainless-steel screw adjusted the electrode separation distance to the thickness of the resin wafer. EIS was conducted with a 1 mA perturbation in the frequency range of 100 kHz to 1 Hz and the high frequency resistance from the Nyquist plot was used to calculate the conductivity with eqn (1),

$$\kappa = \frac{t}{A \cdot R} \qquad (1)$$

where κ denotes the ionic conductivity of the RW, t denotes the wafer thickness, A denotes the RW surface area, R is the measured resistance value. Conductivity was measured in NaCl solutions that ranged from 0.1 g L^{-1} to 29.2 g L^{-1}. The solutions from 3.4 g L^{-1} to 29.2 g L^{-1} were prepared by serial dilution while the final 0.1, 0.4 and 0.5 g L^{-1} solutions were prepared individually.

Porosity

Macroporosity of the RWs was measured using blue dextran (Sigma Aldrich D5751). RWs were fully saturated with Milli-Q water, subject to vacuum filtration, and immersed in 5 g L^{-1} blue dextran. After 5 minutes, the excess blue dextran (free liquid) was removed from the surface by blot drying using a Kimwipe, and each RW was thoroughly rinsed with Milli-Q water. The concentrations of blue dextran in the initial and rinse solutions were measured by absorbance at 620 nm using UV-vis (UV-1800, Shimadzu, Columbia, MD) and used to calculate the free-liquid-void-space (FLVS) and porosity (Φ) as shown in eqn (2) and (3),

$$V_{\text{FLVS}} \ (\text{mL}) = \frac{C_{\text{final}} \times V_{\text{final}}}{C_{\text{initial}}} \qquad (2)$$

$$\Phi \ (\%) = \frac{V_{\text{FLVS}}}{l \times w \times h} \times 100 \qquad (3)$$

where C_{initial} and C_{final} are the blue dextran concentrations in the initial and rinse solutions, respectively, w is the width of the wafer, l is the length of the wafer, and h is the height of the wafer.

This journal is © The Royal Society of Chemistry 2020

Mol. Syst. Des. Eng., 2020, **5**, 922–935 | **925**

RW ion-exchange capacity (IEC) calculation

The theoretical IEC of the RWs, by weight and volume, was calculated using eqn (4) and (5), respectively. The IEC values are essentially a weighted average of the individual IEC values of each component added to the RW. The IEC by weight is normalized by the mass of the RW whereas the IEC by volume is normalized by the volume of solids in the RW.

$$IEC \text{ (by weight)}$$
$$= \frac{IEC_{CER} \times m_{CER} + IEC_{AER} \times m_{AER} + IEC_{binder} \times m_{binder}}{m_{RW}}$$
$$(4)$$

$$IEC \text{ (by volume)} = \frac{IEC \text{ (by weight)} \times m_{RW}}{V_{RW} \times (1 - \Phi)} \quad (5)$$

IEC_{CER}, IEC_{AER}, IEC_{binder} denote the IEC values of the CER, AER, and binder(s), respectively, in milliequivalents (meq) per gram. m_{CER}, m_{AER} and m_{binder}, m_{RW} denote the masses of the CER, AER, and binder and total RW, respectively. V_{RW} denotes the volume of the RW, and Φ denotes the RW porosity. The NaCl (porosigen) added to the RW during manufacturing was dissolved by immersing the RWs in DI water and was not considered in the IEC calculation.

SEM and EDX mapping

The cross-sectional morphology of the Janus RWs was observed under a field emission-scanning electron microscope (Quanta™ 3D DualBeam™ FEG FIB/SEM) at an operating voltage of 20 kV while maintaining a working distance of 10 mm. To increase conductivity during imaging, the samples were affixed to SEM mounts with conductive carbon tape and coated with less than 1 nm of platinum using a sputter coater (EMS550X). Elemental analysis was carried out using an energy dispersive X-ray spectrophotometry instrument (TEAM™ Pegasus EDS-EBSD).

EDI measurements

RW-EDI experiments were conducted using a homemade ED stack consisting of a stainless-steel cathode and dimensionally-stable anode (DSA). Ion-exchange membranes (active area = 14 mm^2) were arranged in an alternating pattern to create diluate compartments (~2.5 mm thick) containing RWs and concentrate compartments (~0.7 mm thick) for a total of 4 cell pairs. Experiments were conducted in batch mode using an initial concentration of 5000 g L^{-1} NaCl for both the feed and concentrate solutions, a feed flow rate of 19 mL min^{-1}, a concentrate flow rate of 38 mL min^{-1}, and cell voltage of 1 V cell pair^{-1}.

Ion-chromatography analysis

Cl$^-$ concentrations were measured with ion chromatography (882 Compact IC plus; Metrohm, Riverview, FL) equipped with chemical and CO$_2$ suppression systems. Analyses were performed with Metrosep A Supp 5 150/4.0 analytical and guard columns, 3.2 mM Na$_2$CO$_3$/1.0 mM NaHCO$_3$ as the eluent, a flow rate of 0.7 mL min^{-1}, and 20 μL sample loop and injection volumes.

Assessing water-splitting of Janus bipolar RW samples in 4-point electrochemical cell setup

Water-splitting current–voltage relationships of the Janus bipolar RW samples were assessed using a home-built 2 compartment, 4-point electrochemical cell setup.[30–32] The active area for the RW samples and bipolar membrane in the cell was 1.27 cm^2. The cell consists of 2 Pt/Ir working electrode meshes, one in each compartment, and Ag/AgCl reference electrodes with Luggin capillaries intimately pressed against the membrane/RW interfaces. The supporting electrolyte in each compartment was aqueous 0.5 M Na$_2$SO$_4$, and this solution was mixed under constant stirring using a PTFE coated stir bar. The potential drop across the sample was controlled to be 2 V, and the steady-state current response was measured.

Results and discussion

Manufacturing of single ion-conducting RWs

Fig. 2A depicts the design of single ion-conducting RWs that solely feature anion exchange or cation exchange material. The anion conducting RWs were constructed with AERs and an AEI binder (QAPSf) while the cation conducting RWs were constructed with CER and a CEI binder (SPEEK). Pairing a similar charged ion-exchange resin and polymer electrolyte binder creates a high concentration of fixed charge density in the RW material. AEI–AER wafers and CEI–CER RWs have high concentrations of fixed cations and anions, respectively. The high concentration of fixed charges facilitates passage of the counterion (*i.e.*, anions in the case of AEI–AER or cations in the case of CEI–CER) while minimizing transport of the co-ion (*i.e.*, cations for AEI–AER or anions for CEI–CER) due to Donnan exclusion.[35]

Fig. 2B illustrates the manufacturing process of the single ion-conducting RWs. AEI and CEI binders were prepared as described elsewhere.[30] The ^{1}H NMR of the AEI and CEI binders and IEC values of the RWs are presented in Fig. S1a–c† and Table 1. AERs and CERs were vacuum dried at room temperature for 30 minutes prior to use to remove moisture. The ionomer was dissolved to form a 14 wt% concentration in *N*-methyl-2-pyrrolidone (NMP) solvent. The ionomer solution was mixed with the ion-exchange resins and sodium chloride (a sacrificial porosigen) in a 2 : 2.4 : 1 ratio and then cast into a foil-lined stainless-steel mold. The mold was dried in an oven at 60 °C for 12 hours to remove residual solvent and then hot pressed at 2 metric ton load for 125 °C for 1.5 hours for the CEI–CER or 150 °C for 2 hours for the AEI–AER. The RWs were cooled under the 2-metric ton load before removing from the molds and then immersed in DI
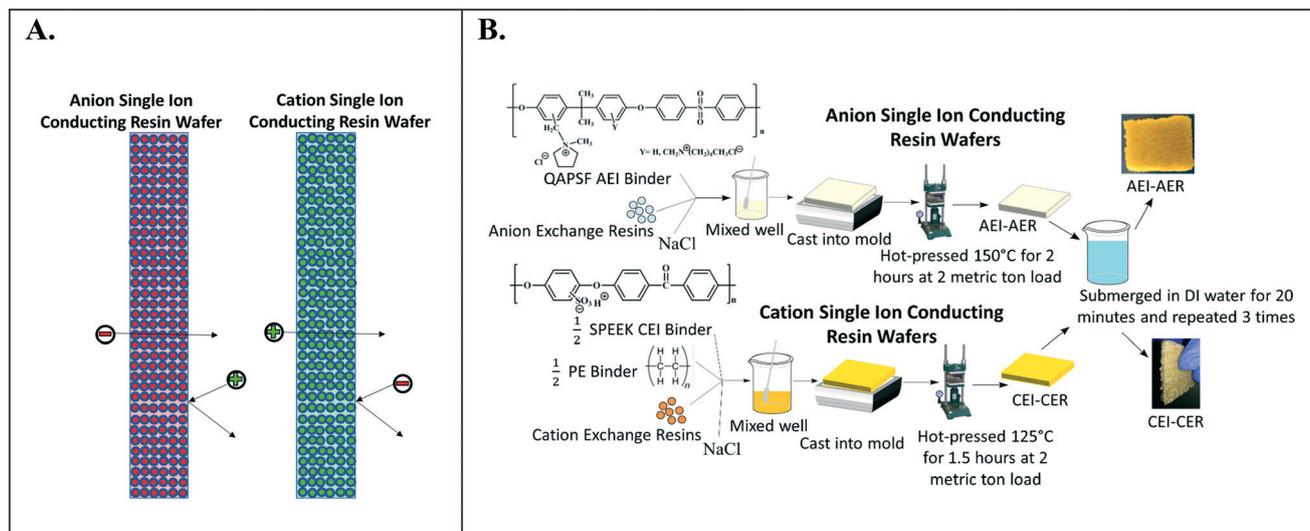
Fig. 2 (A) Illustration of single ion-conducting RWs. (B) Manufacturing scheme for single anion- and single cation-conducting RWs.

water three times for 20 minutes to dissolve the porosigen (*i.e.*, NaCl).

In our previous work,[30] SPEEK based CEI binder produced mechanically stable RWs with a CER–AER mixture and AER only. However, the CEI binder with the CER only resulted in a mechanically fragile RW (see Fig. S2†) indicating that binder and ion-exchange resin compatibility are important properties for making robust RWs. Our previous work showed that quality RWs could not be produced from perfluorosulfonic acid binders (*e.g.*, Nafion®), and sulfonated polystyrene binders, suggesting that it was necessary to modify the manufacturing procedure for the CER RW by blending PE binder with the SPEEK ionomer solution (1:1 mass ratio). This manufacturing procedure produced a robust, free-standing cation-exchange RW shown in Fig. 2B.

Ionic conductivity and material properties of single ion-conducting RWs

The ionic conductivity values of the single ion-conducting RWs were measured in a two-point static conductivity cell at various NaCl concentrations (Fig. 3A). The single ion-conducting RWs were benchmarked against the conventional mixed RW with PE binder and NaCl solution conductivities. Duplicate measurements were performed for the ionomer

RWs, and the error bars in Fig. 3A represent the absolute difference between the mean of both measurements. Both of the single ion-conducting RWs exhibited higher conductivities than the benchmark RW that featured mixed AER and CER with PE binder. Porosity measurements (Table 1) indicated that the single ion-conducting RWs were as porous as the benchmark RW that has been used in numerous EDI demonstrations.[15,16]

The AEI–AER RW (indicated by the black squares in Fig. 3A) displayed higher ionic conductivity in comparison to CEI–CER RW (indicated by the blue diamonds in Fig. 3A) and mixed RW (indicated by the green triangles in Fig. 3A) featuring either AER or CER due to a higher ionic mobility for Cl^- over Na^+ in dilute water streams[36] (7.91×10^{-4} cm^2 s^{-1} V^{-1} for Cl^- and 5.194×10^{-4} cm^2 s^{-1} V^{-1} for Na^+ – *i.e.*, about 50% higher for chloride). Ionic mobility represents the migration rate of an ion in the presence of an applied electric field, and it is proportional to the diffusion coefficient normalized to the thermal energy of the system.

Fig. 3B presents the ionic conductivity of the RW samples normalized to their IEC values. Ionic conductivity is linearly dependent on the concentration of fixed charger carriers in the ion-exchange material.[37] Thus, a material with a higher IEC would result in higher ionic conductivity. The AEI–AER still displayed the highest ionic conductivity when normalized to IEC at low NaCl concentrations. The ionic conductivity for single ion-conducting RWs is attributed to two factors: i) counterion migration along the polymer in the ion-exchange resin and ionomer binder and ii) ionic migration of the supporting electrolyte (*i.e.*, NaCl) dissolved in the RW sample. By normalizing the ionic conductivity to the IEC, it is clear that the AEI–AER displays greater ionic conductivity because the counterion, Cl^-, has a higher ionic mobility than Na^+.

In the context of most electrochemical separation platforms, deionization occurs by transport of anions and

Table 1 Ion exchange capacity (IEC) and porosity of RWs

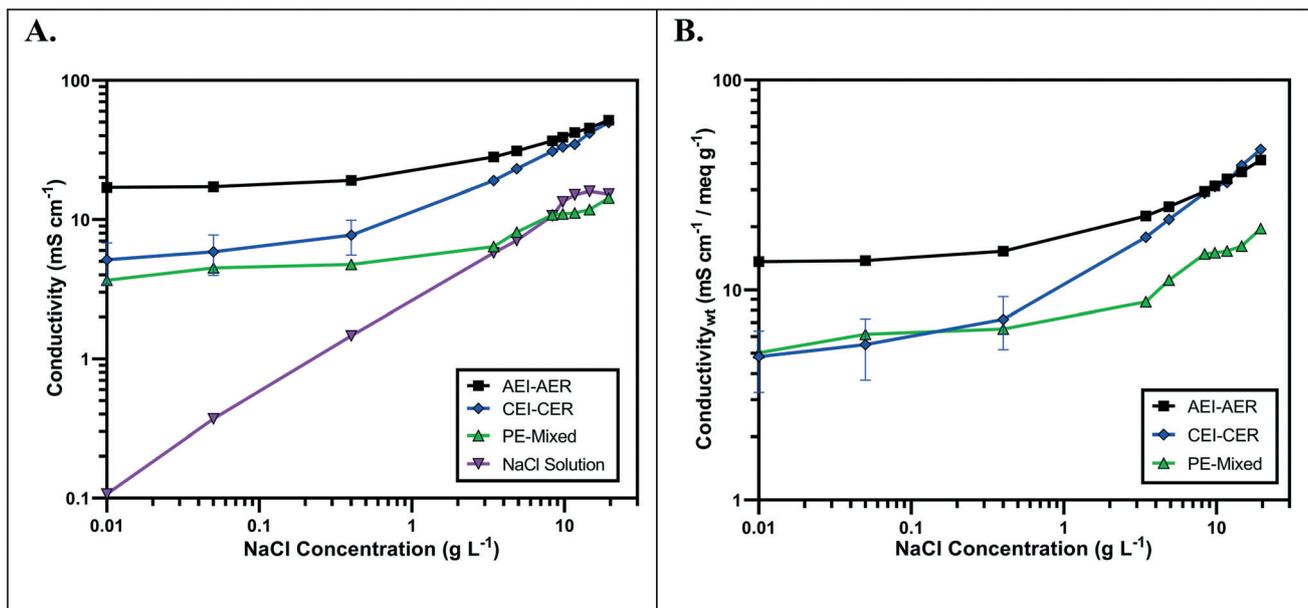| Resin wafer type	IEC (meq g^{-1})	IEC (meq mL^{-1})	Porosity (%)
CEI–CER	1.07	1.00	13.5 ± 1.6
AEI–AER	1.25	0.99	16.6 ± 1.5
AEI-mixed	1.36	0.96	18.6 ± 3.4
AEI–CER	1.50	0.99	13.0 ± 1.9
PE-mixed	0.73	0.82	15.7 ± 1.2
Symmetric Janus with catalyst	0.99	1.05	16.7 ± 3.5
Symmetric Janus without catalyst	1.14	0.91	15.6 ± 3.2

Fig. 3 (A) Ionic conductivity of single ion-conducting RWs at various NaCl concentrations. (B) Ionic conductivity normalized to ion-exchange capacity at various NaCl concentrations. Error bars in these plots represent the absolute difference (n = 2) from the average for the ionomer RWs.

cations across an AEM or CEM, respectively. The rate of ion removal is dependent upon the rate of delivery of ions to these interfaces, and thus, the ionic mobility values in the aqueous phase and ion-exchange resin bed are important descriptors for EDI transport. Because of iso-neutrality constraints, the ratio of cations to anions (assuming both have the same valence number) must be equivalent in the diluate and concentrate chambers. Hence, the rate of both anion and cation removal from the diluate chamber is limited by the slowest moving ion. Based on the ionic conductivity results from single ion-conducting RWs, it seems that improving deionization of NaCl from water with RW-EDI requires a strategy to promote Na$^+$ conductivity. Since ionic mobility is an intrinsic property of the ion itself, an alternative strategy for further research would be to increase the IEC of the CER in order to improve Na$^+$ conductivity and the overall efficiency of EDI. Other strategies, such as molecular engineering of the RW materials (e.g., percolating pathways of ionic channels),[38] may also be another effective means for promoting Na$^+$ conductivity.

Manufacture of Janus bipolar RWs and incorporation of a water dissociation catalyst

The development of single ion-conducting RWs allowed for the manufacture of Janus bipolar RWs with adjacent cation and anion exchange layers. Two manufacturing schemes were devised to incorporate a planar layer of a water dissociation catalyst into both symmetric and asymmetric designs of the Janus bipolar RW. It was posited that the addition of water dissociation catalyst would promote water-splitting during EDI operation and enable greater current flow at lower

concentrations of dissolved salt in the diluate chamber. The symmetric Janus bipolar RW contains equivalent thicknesses of the anion and cation exchange layers (illustrated in Fig. 4A) while the asymmetric variant (Fig. 4B) was devised by spraycoating a thin cation exchange layer onto a relatively thick anion exchange layer. Although it was beyond the scope of this work, the manufacturing process for making Janus bipolar RWs is further amenable, so it would be possible to reverse the asymmetric design and create a larger cation exchange layer (Fig. 4C) or place multiple layers of the water dissociation catalyst in the RW to accelerate the water-splitting phenomenon (Fig. 4D). The relative thickness of the cation and anion exchange layers (i.e., the distances that OH$^-$ and H$^+$ must traverse in order to reach membrane surfaces) can thus be manipulated through the Janus bipolar RW manufacture process to control the pH values of the diluate and concentrate chambers. The possibilities for controlling the solution pH through the use of materials with modified morphologies will be explored in the future and with niche separation applications such as silica and organic acid separation.

Fig. 5A illustrates the layering method used to manufacture a symmetric Janus bipolar RW. In this approach, the initial CEI–CER layer was prepared as described in Fig. 2B; however, the final submersion in DI water was omitted. After preparing the CEI–CER RW, a uniform layer of aluminum hydroxide (Al(OH)$_3$) nanoparticles (10 wt% of particles suspended in DI water) was applied on to the CEI–CER layer with a final loading of 0.034 g cm^{-2}. The catalyst layer was deposited in three applications and allowed to dry for 30 minutes after each application. The CEI–CER layer was inserted into a foil-lined stainless-steel mold, and the AEI–AER mixture described in Fig. 2B was layered on top. The symmetric Janus bipolar RW was dried at
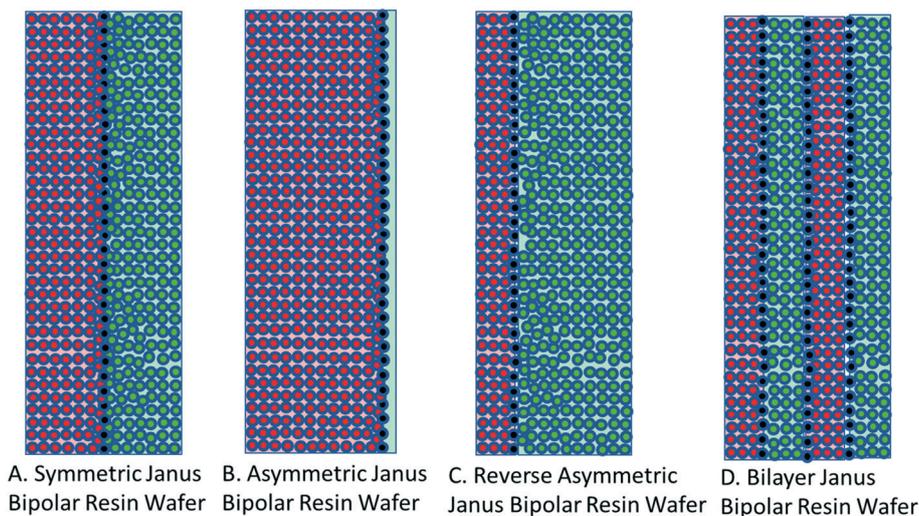
A. Symmetric Janus Bipolar Resin Wafer B. Asymmetric Janus Bipolar Resin Wafer C. Reverse Asymmetric Janus Bipolar Resin Wafer D. Bilayer Janus Bipolar Resin Wafer

Fig. 4 Cross-sectional views of (A) symmetric and (B) asymmetric Janus bipolar resin wafers used in this report and concepts of a (C) reversed asymmetric and (D) bilayer Janus bipolar resin wafer.
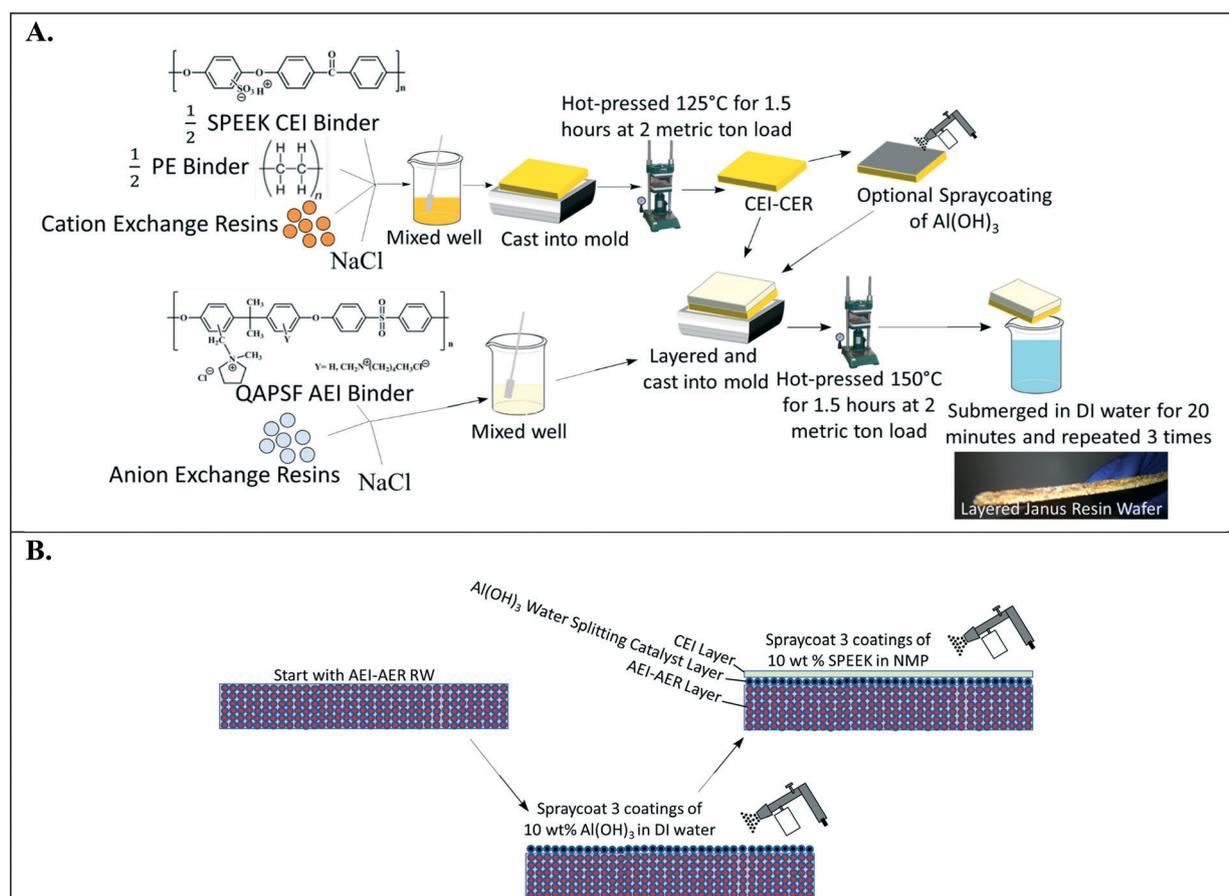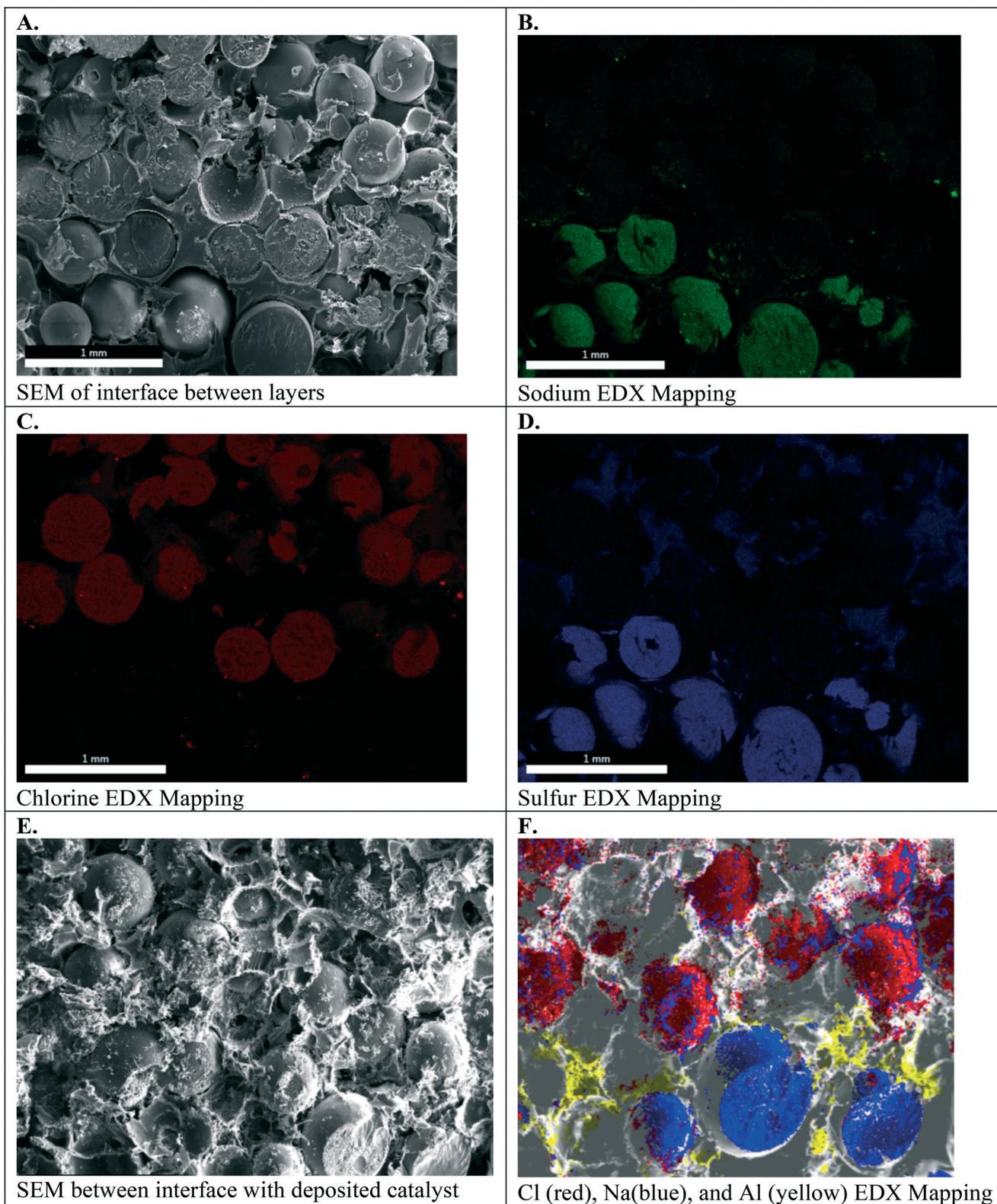

Fig. 5 (A) Manufacturing scheme for symmetric Janus bipolar RW with optional inclusion of a water dissociation catalyst ($Al(OH)_3$ nanoparticles). (B) Manufacturing scheme for an asymmetric Janus bipolar RW with optional inclusion of a water dissociation catalyst.

60 °C for 12 hours, hot pressed at 150 °C for 1.5 hours, and allowed to cool under load to room temperature. The final symmetric Janus bipolar was submerged in DI water for a total of 1 hour, during which the water was exchanged three times to remove the porosigen. A photo of the symmetric Janus bipolar RW is shown in Fig. 5A. The darker and lighter sides of the RW correspond to the cation and anion exchange layers, respectively.

A.

SEM of interface between layers

B.

Sodium EDX Mapping

C.

Chlorine EDX Mapping

D.

Sulfur EDX Mapping

E.

SEM between interface with deposited catalyst

F.

Cl (red), Na(blue), and Al (yellow) EDX Mapping

Fig. 6 Electron micrographs of symmetric Janus bipolar RW interface without a catalyst (A) image with no EDX mapping. (B) Chlorine (Cl) EDX map (anion exchange layer). (C) Sodium (Na) EDX map (cation exchange layer). (D) Sulfur EDX map. Electron micrographs of symmetric Janus bipolar RW interface (E) image without EDX mapping and (F) EDX mapping of Cl, Na, and aluminum (Al).

The second manufacturing method for preparing the asymmetric Janus bipolar RW is shown in Fig. 5B. Unlike the symmetric RW, the AEI–AER was first prepared as detailed in Fig. 2B, omitting the water immersion step. Next, the water dissociation catalyst was added in the same fashion as described for Fig. 5A. Rather than applying the oppositely charged CEI–CER on top of the AEI–AER with a water dissociation catalyst, a thin film of SPEEK ionomer was deposited through three applications of spray deposition (10 wt% SPEEK in NMP) with a final loading of 0.14 g cm^{-2}. The rationale for selecting the asymmetric Janus bipolar RW variant was based on i) the previous ionic conductivity results, which showed that the AEI–AER had the highest ionic conductivity (Fig. 3A), and ii) the straightforward nature of this manufacturing procedure, which involved fewer processing steps to incorporate a bipolar junction and water dissociation catalyst.

Fig. 6A–D. present the electron micrographs, with and without EDX mapping, at the interface between cation exchange and anion exchange groups in the symmetric Janus bipolar RW that did not contain a water dissociation catalyst. Fig. 6A confirms successful integration of the AEI–AER and CEI–CER; the two porous layers are in contact with each other. Elemental mapping for sodium and chlorine in these micrographs, Fig. 6B and C respectively, revealed separate and distinct cation and anion exchange layers (i.e., an abrupt, oppositely charged molecular bipolar junction interface). Sodium is the counterion to the tethered sulfonate groups in the CEI–CER material, while chloride is the counterion for the tethered quaternary ammonium groups used in the AEI–AER. Fig. 6D shows the EDX mapping for sulfur, which is present as sulfonic groups CER and CEI, and as a minor component in AEI due to the poly(arylene ether sulfone) backbone. As a result, a stronger signal for sulfur is evident in the CEI–CER layer in comparison to the AEI–AER layer.

When manufacturing the symmetric Janus bipolar RW, it was discovered that the mechanical-thermal lamination press time was a critical parameter. EDX mapping indicated that excessive press times, such as 2 hours or greater, resulted in mixing of CEI and AEI binders and precluded the formation of an abrupt bipolar junction layer. A 1.5 hour press time at 150 °C was determined to be ideal because it yielded an intimate, but distinct, bipolar junction. Although quantifying the effects of press time on the interface were outside the scope of this work, measuring the electrochemical properties of the bipolar junctions could provide a better understanding of the structure, property, and performance relationships for these materials. In this study, the focus was limited to adjoining the two different RWs into one mechanically robust RW (i.e., the symmetric Janus bipolar RW sample). With a successful manufacturing scheme in place, the Janus bipolar RW with a water dissociation catalyst was prepared and imaged with SEM and EDX mapping (Fig. 6E and F). From these SEM images, it is evident that the sodium and chlorine layers are separated by an aluminum layer at the interface.

Ionic conductivity of Janus bipolar RWs

Fig. 7 presents the ionic conductivity values of the symmetric and asymmetric Janus bipolar RWs with and without the Al(OH)$_3$ water dissociation catalyst. The Janus RWs were benchmarked against the AEI–AER, which was previously found to be the most conductive RW (Fig. 3A). Both the symmetric and asymmetric Janus RWs without the water dissociation catalyst demonstrated lower ionic conductivities in comparison to the AEI–AER. The decreased conductivity for the layered Janus RW was expected because control experiments with RWs featuring an AEI binder and CER only or a mixture of CER–AER had lower ionic conductivity (Fig. S3†). The lower ionic conductivity of the RW samples containing CER was ascribed to the lower ionic mobility of the Na$^+$ that is primarily transferred by the CER.

The addition of the Al(OH)$_3$ water dissociation catalyst into the symmetric and asymmetric Janus bipolar RW samples increased their ionic conductivity values to those comparable with the AEI–AER RW at low NaCl concentrations (<3 g L^{-1}). At higher NaCl concentrations (>3 g L^{-1}), the Janus bipolar RWs had slightly higher ionic conductivity values when compared to the AEI–AER. The increase in ionic conductivity with the addition of Al(OH)$_3$ into the RW was unexpected because the Al(OH)$_3$ does not contain any formal ionic charges. However, Al(OH)$_3$ can accept an OH$^-$ from solution to form an ionic pair between Al(OH)$_4^-$ and H$^+$. If these ionic pairs exist in small populations on the nanoparticle surfaces, they could potentially augment the ionic conductivity of the RW sample. To further explore this hypothesis, Al(OH)$_3$ nanoparticle suspensions were prepared with various concentrations, and the solutions' ionic conductivities were measured using a conductivity probe (Fig. S4†). At 0.2 M, Al(OH)$_3$ nanoparticle suspension exhibited a moderate ionic conductivity value of 0.53 mS cm^{-1} suggesting the formation of Al(OH)$_4^-$ on the nanoparticle surface. It is difficult to quantify the exact concentration of the nanoparticles in the RW samples, but it is lower than 0.2 M (which was measured as suspension in DI water), and the addition of the Al(OH)$_3$ nanoparticles into the Janus bipolar RW samples resulted in a nearly two-fold increase in ionic conductivity (i.e., 7 to 10 mS cm^{-1}) in comparison to the non-catalyst containing samples. It is also unlikely that the increase in ionic conductivity was attributed to water-splitting because the cell voltage during electrochemical impedance spectroscopy was small (<1 mV). While the formation of a surface charge on the Al(OH)$_3$ nanoparticles is plausible, further investigations are warranted to better understand the increase in RW ionic conductivity with a water dissociation catalyst.

Water-splitting characterization of Janus bipolar RWs in a 4-pt cell setup

Most studies that report water-splitting in EDI draw this conclusion from measuring shifts in the effluent pH. However, a 4-point, two-compartment cell is often used for
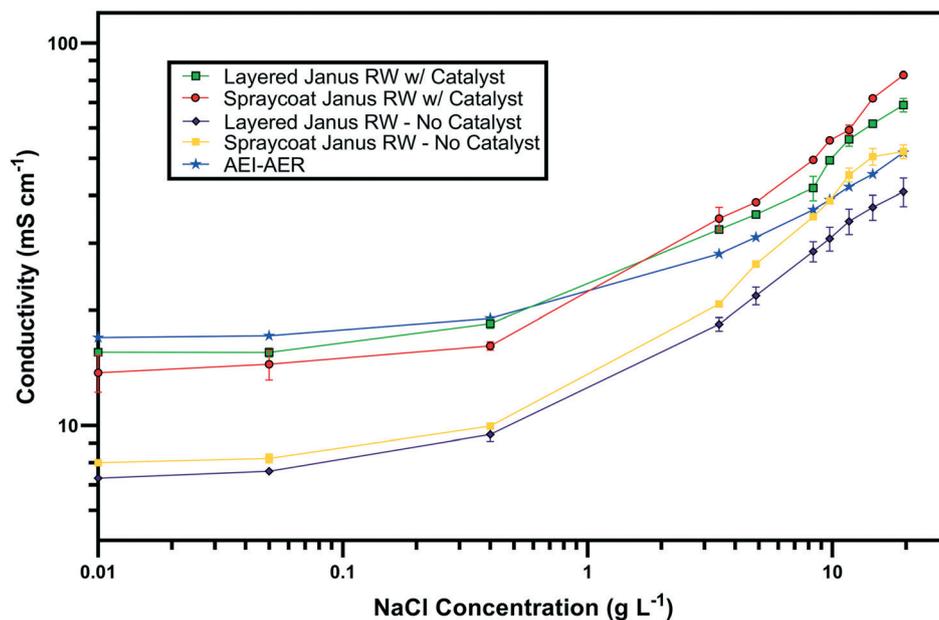
This journal is © The Royal Society of Chemistry 2020

Mol. Syst. Des. Eng., 2020, 5, 922–935 | 931

Fig. 7 Ionic conductivity of symmetric and asymmetric Janus bipolar RWs with and without water dissociation catalyst. Error bars represent absolute difference (n = 2) from the average of measurements.

assessing the water-splitting capabilities of BPMs, a class of ion-exchange materials used for generating H^+ and OH^-, through acquisition of steady-state polarization behavior.[21,32] Fig. 8 reports the current response for a 2 V potential drop across the Janus bipolar RW samples with and without a water dissociation catalyst in a homemade 4-point, two-compartment cell that features platinum–iridium (Pt/Ir) mesh working electrodes and two silver–silver chloride (Ag/AgCl) reference electrodes. The supporting electrolyte for the

experiments was 0.5 M sodium sulfate (Na_2SO_4), and the 2 V potential drop across the RW samples was selected because it was well-above the minimum thermodynamic potential (0.83 V)[32] to split water into H^+ and OH^-. Fig. 8 clearly shows that the addition of a water dissociation catalyst enhanced the current response by at least a factor of two (and in the case of symmetric Janus RW, it was over 100). The high ionic conductivities and exceptional water-splitting capabilities of the Janus bipolar RWs suggested that these materials would be good candidates for additional investigation in an EDI process.
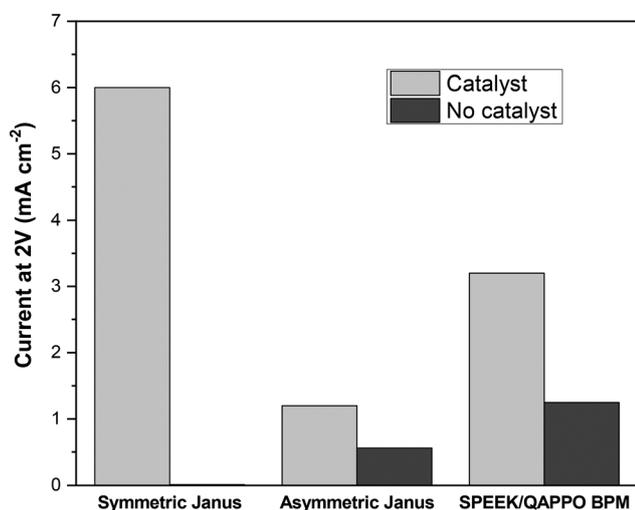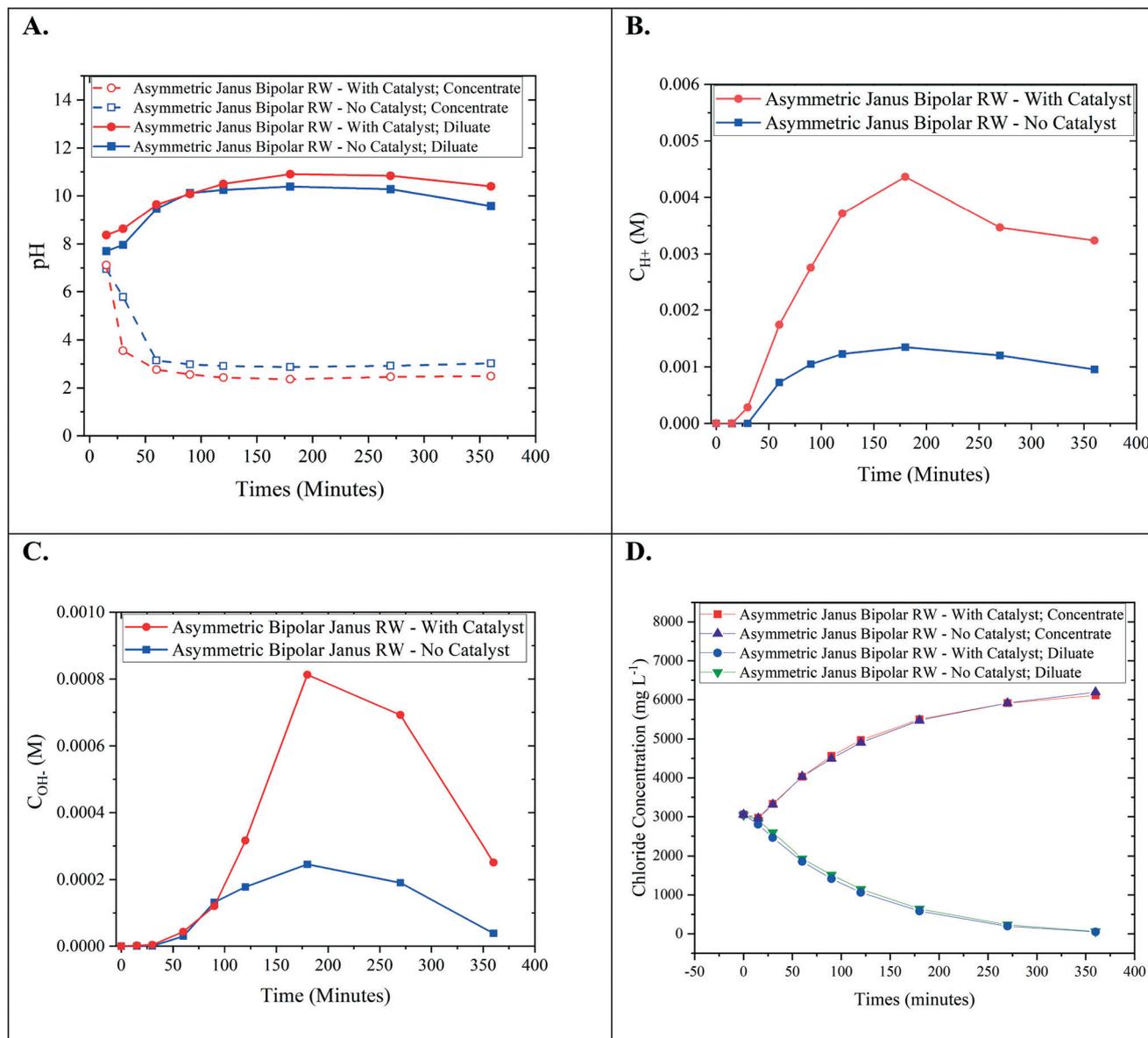
EDI demonstrations

Bench-scale RW-EDI experiments were conducted in order to evaluate the water-splitting capabilities of an asymmetric Janus bipolar RW featuring a water dissociation catalyst. Control EDI experiments were also performed with an asymmetric Janus bipolar RW that did not contain the $Al(OH)_3$ water dissociation catalyst. The asymmetric Janus bipolar RW was selected over the symmetric Janus bipolar RW because the manufacturing procedure was more simple and produced more mechanically robust RWs. EDI demonstrations were performed in batch mode with synthetic aqueous NaCl solutions (initial concentration for the diluate and concentrate chambers was 5 g L^{-1}). The diluate and concentrate solutions were continuously recirculated for the duration of each EDI demonstration. The pH of diluate and concentrate streams were monitored throughout the experiment, and the results are presented in Fig. 9A. In this figure, the pH of the diluate stream increased while the pH of the concentrate stream decreased. Changes in pH are consistent with water-splitting that yields H^+ and OH^-. This phenomenon has been documented in the literature for various applications of EDI processes by

Fig. 8 Current response for a 2 V drop across Janus bipolar RW samples with and without a water dissociation catalyst (left and middle bar graphs). For reference, measurements were also performed with homemade BPM with and without a water dissociation catalyst ($Al(OH)_3$). The measurements were carried out in a homemade 4-point cell with two reference electrodes measuring the potential drop across the RW/BPMs and Pt/Ir mesh working electrodes in 0.5 M Na_2SO_4.

Fig. 9 (A) pH of concentrate and diluate chambers during EDI demonstration *versus* recirculation time for asymmetric Janus bipolar RW with and without a water dissociation catalyst. (B) Proton concentration in concentrate chamber during the EDI demonstration. (C) Hydroxide concentration in diluate chamber during the EDI demonstration. (D) EDI performance as measured by the removal of chloride salt anions from the diluate chamber to the concentrate chamber with an asymmetric Janus bipolar RW with and without a water dissociation catalyst.

monitoring solution pH.[6,7,39,40] Notably, the relative changes in pH values were higher for the experiment that used a RW featuring a water dissociation catalyst. To the best of our knowledge, no EDI process has incorporated a water dissociation catalyst in the ion-exchange resin bed. The pH data presented in Fig. 9A shows that the incorporation of a catalyst improved the water-splitting rate.

Owing to the small changes on a logarithmic scale, pH values were converted to H^+ in the concentrate and OH^- in the diluate (Fig. 9B and C). From these plots, it is clear that the increase in acidity in the concentrate and alkalinity in the diluate is greater by a factor of 3–4 for a Janus bipolar RW sample containing a water dissociation catalyst. The reduction in diluate alkalinity over time resulted from the

depletion of Cl^- (near 80% removal) from the diluate chamber (Fig. 9D) and thus, continual deionization required removal of accumulated OH^- in the diluate chamber through the AEM to maintain electrical current flow in the EDI.

Aside from changes in pH, desalination performance was evaluated for asymmetric Janus bipolar RWs both with and without water splitting catalyst. Fig. 9D shows that as expected in both cases, the Cl^- concentration in the diluate compartment decreased with time while the Cl^- concentration in the concentrate compartment increased with time. The Cl^- concentration profiles for wafers with and without the water splitting catalyst were not significantly different, which suggest that the inclusion of the catalyst does not necessarily facilitate Na^+ or Cl^- ion transport. This

This journal is © The Royal Society of Chemistry 2020

Mol. Syst. Des. Eng., 2020, **5**, 922–935 | **933**

can be attributed to the 3–7 higher ion mobility for H^+ and OH^- in comparison to Na^+ and Cl^- in water,[36] which have been reported to parallel the trends in ion-exchange resins.[41]

In summary, the EDI tests showed that asymmetric Janus bipolar RWs featuring $Al(OH)_3$ as a water dissociation catalyst promoted greater water-splitting in comparison to similar Janus bipolar RWs that lack the catalyst but did not affect Cl^- deionization. Overall, these results imply that Janus RW materials may be an appropriate substitute for EDI processes that utilize BPMs, analogous to BPM electrodialysis but without the requirement of having to use high feed concentrations to minimize spacer channel resistances.

Conclusions

A new class of single ion-conducting RWs was developed to foster cation or anion conduction. Ionic conductivity measurements demonstrated the AEI–AER RW was the most conductive RW in dilute NaCl solutions reported to date (17 ± 0.26 mS cm^{-1} in 0.1 g L^{-1} NaCl). Further, the new single ion-conducting materials revealed that ion exchange resins (and not only the ionomer binder) provide substantial contribution to the overall RW conductivity, and the current commercially available CER is less conductive than the AER. This finding motivates future research to pursue solutions that are focused on improving cation conductivity within RWs and molecularly engineered percolation pathways with the overall goal of promoting more efficient electrochemical separations.

Additionally, Janus bipolar RWs were explored by the development of the single ion-conducting of RWs. The addition of a water dissociation catalyst into a molecularly intimate polycation–polyanion bipolar junction interfaces located in porous RW materials was investigated for the first time. The water dissociation catalyst enhanced the conductivity of the RW, and these Janus wafers rivaled the conductivity of the most conductive single ion-conducting RW (AEI–AER). The EDI demonstration of the asymmetric Janus RW showed that these materials can be utilized to modify the solution pH and suggest that pH control with RW material could be useful to enable future electrodeionization separation technologies that may compete with bipolar membrane electrodialysis.

Conflicts of interest

There are no conflicts of interest to declare.

Acknowledgements

References

1 X. Su, K.-J. Tan, J. Elbert, C. Ruttiger, M. Gallei, T. F. Jamison and T. A. Hatton, Asymmetric Faradaic systems for selective electrochemical separations, *Energy Environ. Sci.*, 2017, **10**(5), 1272–1283.

2 National Academies of Sciences, E., and Medicine, *A Research Agenda for Transforming Separation Science*, The National Academies Press, Washington, DC, 2019, p. 114.

3 V. A. Shaposhnik and K. Kesore, An early history of electrodialysis with permselective membranes, *J. Membr. Sci.*, 1997, **136**(1–2), 35–39.

4 F. DiMascio, J. Wood and J. M. Fenton, Continuous electrodeionization. Production of high-purity water without regeneration chemicals, *Electrochem. Soc. Interface*, 1998, **7**(3), 26–29.

5 R. Decker, Deionization overview, *Ultrapure Water*, 2010, **27**(9), 37–39.

6 L. Alvarado and A. Chen, Electrodeionization: Principles, strategies and applications, *Electrochim. Acta*, 2014, **132**, 583–597.

7 O. Arar, U. Yuksel, N. Kabay and M. Yuksel, Various applications of electrodeionization (EDI) method for water treatment. A short review, *Desalination*, 2014, **342**, 16–22.

8 T. J. Welgemoed and C. F. Schutte, Capacitive Deionization Technology: An alternative desalination solution, *Desalination*, 2005, **183**(1–3), 327–340.

9 Y. Oren, Capacitive deionization (CDI) for desalination and water treatment — past, present and future (a review), *Desalination*, 2008, **228**(1–3), 10–29.

10 P. M. Biesheuvel and A. van der Wal, Membrane capacitive deionization, *J. Membr. Sci.*, 2010, **346**(2), 256–262.

11 L. Weinstein and R. Dash, Capacitive Deionization: Challenges and Opportunities, *Int. Desalin. Water Reuse Q.*, 2013, 34–37.

12 D. Deng, E. V. Dydek, J.-H. Han, S. Schlumpberger, A. Mani, B. Zaltzman and M. Z. Bazant, Overlimiting Current and Shock Electrodialysis in Porous Media, *Langmuir*, 2013, **29**(52), 16167–16177.

13 D. Deng, W. Aouad, W. A. Braff, S. Schlumpberger, M. E. Suss and M. Z. Bazant, Water purification by shock electrodialysis: Deionization, filtration, separation, and disinfection, *Desalination*, 2015, **357**, 77–83.

934 | *Mol. Syst. Des. Eng.*, 2020, **5**, 922–935

This journal is © The Royal Society of Chemistry 2020

14 S. Voskian and T. A. Hatton, Faradaic electro-swing reactive adsorption for CO_2 capture, *Energy Environ. Sci.*, 2019, **12**, 3530–3547.

15 S. Datta, M. P. Henry, Y. J. Lin, A. T. Fracaro, C. S. Millard, S. W. Snyder, R. L. Stiles, J. Shah, J. Yuan, L. Wesoloski, R. W. Dorner and W. M. Carlson, Electrochemical CO2 Capture Using Resin-Wafer Electrodeionization, *Ind. Eng. Chem. Res.*, 2013, **52**(43), 15177–15186.

16 S.-Y. Pan, S. W. Snyder, H.-W. Ma, Y. J. Lin and P.-C. Chiang, Development of a Resin Wafer Electrodeionization Process for Impaired Water Desalination with High Energy Efficiency and Productivity, *ACS Sustainable Chem. Eng.*, 2017, **5**(4), 2942–2948.

17 V. M. Palakkal, J. E. Rubio, Y. J. Lin and C. G. Arges, Low-Resistant Ion-Exchange Membranes for Energy Efficient Membrane Capacitive Deionization, *ACS Sustainable Chem. Eng.*, 2018, **6**(11), 13778–13786.

18 W. Walters, R.; Weiser, D. W.; Marek, L. J., Concentration of radioactive aqueous wastes. Electromigration through ion-exchange membranes, *Ind. Eng. Chem.*, 1955, **47**, 61–67.

19 J. Wood, J. Gifford, J. Arba and M. Shaw, Production of ultrapure water by continuous electrodeionization, *Desalination*, 2010, **250**(3), 973–976.

20 C. G. Arges, V. Prabhakaran, L. Wang and V. Ramani, Bipolar polymer electrolyte interfaces for hydrogen-oxygen and direct borohydride fuel cells, *Int. J. Hydrogen Energy*, 2014, **39**(26), 14312–14321.

21 B. Bauer, F. J. Gerner and H. Strathmann, Development of bipolar membranes, *Desalination*, 1988, **68**(2–3), 279–292.

22 M. Ünlü, J. Zhou and P. A. Kohl, Hybrid Anion and Proton Exchange Membrane Fuel Cells, *J. Phys. Chem. C*, 2009, **113**(26), 11416–11423.

23 F. Fu and Q. Wang, Removal of heavy metal ions from wastewaters: a review, *J. Environ. Manage.*, 2011, **92**(3), 407–418.

24 W. Den and C.-J. Wang, Removal of silica from brackish water by electrocoagulation pretreatment to prevent fouling of reverse osmosis membranes, *Sep. Purif. Technol.*, 2008, **59**(3), 318–325.

25 X. Tongwen, Electrodialysis processes with bipolar membranes (EDBM) in environmental protection—a review, *Resour., Conserv. Recycl.*, 2002, **37**(1), 1–22.

26 C. Huang and T. Xu, Electrodialysis with Bipolar Membranes for Sustainable Development, *Environ. Sci. Technol.*, 2006, **40**(17), 5233–5243.

27 T. E. Lister, L. A. Diaz, M. A. Lilga, A. B. Padmaperuma, Y. Lin, V. M. Palakkal and C. G. Arges, Low-Temperature Electrochemical Upgrading of Bio-oils Using Polymer Electrolyte Membranes, *Energy Fuels*, 2018, **32**(5), 5944–5950.

28 H. Strathmann, H. J. Rapp, B. Bauer and C. M. Bell, Theoretical and practical aspects of preparing bipolar membranes, *Desalination*, 1993, **90**(1–3), 303–323.

29 Z. Yan, L. Zhu, Y. C. Li, R. J. Wycisk, P. N. Pintauro, M. A. Hickner and T. E. Mallouk, The balance of electric field and interfacial catalysis in promoting water dissociation in bipolar membranes, *Energy Environ. Sci.*, 2018, **11**(8), 2235–2245.

30 V. M. Palakkal, L. Valentino, Q. Lei, S. Kole, Y. J. Lin and C. G. Arges, Advancing electrodeionization with conductive ionomer binders that immobilize ion-exchange resin particles into porous wafer substrates, *npj Clean Water*, 2020, **3**, 5.

31 M. B McDonald and M. S. Freund, Graphene Oxide as a Water Dissociation Catalyst in the Bipolar Membrane Interfacial Layer, *ACS Appl. Mater. Interfaces*, 2014, **6**(16), 13790–13797.

32 C. Shen, R. Wycisk and P. N. Pintauro, High performance electrospun bipolar membrane with a 3D junction, *Energy Environ. Sci.*, 2017, **10**(6), 1435–1442.

33 A. M. Lopez and J. A. Hestekin, Improved organic acid purification through wafer enhanced electrodeionization utilizing ionic liquids, *J. Membr. Sci.*, 2015, **493**, 200–205.

34 C. G. Arges, J. Parrondo, G. Johnson, A. Nadhan and V. Ramani, Assessing the influence of different cation chemistries on ionic conductivity and alkaline stability of anion exchange membranes, *J. Mater. Chem.*, 2012, **22**(9), 3733–3744.

35 T. Sata, *Ion Exchange Membranes*, Royal Society of Chemistry, 2007.

36 J. Newman and K. E. Thomas-Alyea, *Electrochemical Systems*, 3rd edn, Wiley, 2004.

37 H. Strathmann, A. Grabowski and G. Eigenberger, Ion-Exchange Membranes in the Chemical Process Industry, *Ind. Eng. Chem. Res.*, 2013, **52**(31), 10364–10379.

38 C. G. Arges, Y. Kambe, M. Dolejsi, G.-P. Wu, T. Segal-Pertz, J. Ren, C. Cao, G. S. W. Craig and P. F. Nealey, Interconnected ionic domains enhance conductivity in microphase separated block copolymer electrolytes, *J. Mater. Chem. A*, 2017, **5**(11), 5619–5629.

39 V. V. Nikonenko, A. V. Kovalenko, M. K. Urtenov, N. D. Pismenskaya, J. Han, P. Sistat and G. Pourcelly, Desalination at overlimiting currents: State-of-the-art and perspectives, *Desalination*, 2014, **342**, 85–106.

40 H. Meng, C. Peng, S. Song and D. Deng, Electro-regeneration mechanism of ion-exchange resin in electrodeionization, *Surf. Rev. Lett.*, 2004, **11**(06), 599–605.

41 H. P. Gregor, J. I. Bregman, F. Gutoff, R. D. Broadley, D. E. Baldwin and C. G. Overberger, Studies on ion-exchange resins. Capacity of sulfonic acid cation-exchange resins, *J. Colloid Sci.*, 1951, **6**, 20–32.